

Journal of Sulfur Chemistry



ISSN: (Print) (Online) Journal homepage: www.tandfonline.com/journals/gsrp20

Design, synthesis, and antitubercular evaluation of piperazinyl-pyrazolyl-2- hydrazinyl thiazole derivatives: Experimental, DFT and molecular docking insights

Yuvraj R. Sable, Vishnu A. Adole, Edwin A. Pithawala & Rakesh D. Amrutkar

To cite this article: Yuvraj R. Sable, Vishnu A. Adole, Edwin A. Pithawala & Rakesh D. Amrutkar (10 Feb 2025): Design, synthesis, and antitubercular evaluation of piperazinyl-pyrazolyl-2-hydrazinyl thiazole derivatives: Experimental, DFT and molecular docking insights, Journal of Sulfur Chemistry, DOI: 10.1080/17415993.2025.2461582

To link to this article: https://doi.org/10.1080/17415993.2025.2461582

+	View supplementary material $oldsymbol{\mathcal{C}}$
	Published online: 10 Feb 2025.
Ø,	Submit your article to this journal 🗗
a ^r	View related articles 🗗
CrossMark	View Crossmark data 🗷





Design, synthesis, and antitubercular evaluation of piperazinyl-pyrazolyl-2- hydrazinyl thiazole derivatives: Experimental, DFT and molecular docking insights

Yuvraj R. Sable ^[ba,b], Vishnu A. Adole ^[ba], Edwin A. Pithawala^c and Rakesh D. Amrutkar^d

^aResearch Centre in Chemistry, Mahatma Gandhi Vidyamandir's Loknete Vyankatrao Hiray Arts, Science and Commerce College, Nashik, India; ^bDepartment of Chemistry, Dr. Patangrao Kadam Mahavidyalaya Ramanandanagar (Burli), Palus, India; ^cDepartment of Microbiology, Silver Oak Institute of Science, Silver Oak University, Ahmedabad, India; ^dDepartment of Pharmaceutical Chemistry, K. K. Wagh College of Pharmacy Panchavati. Nashik. India

ABSTRACT

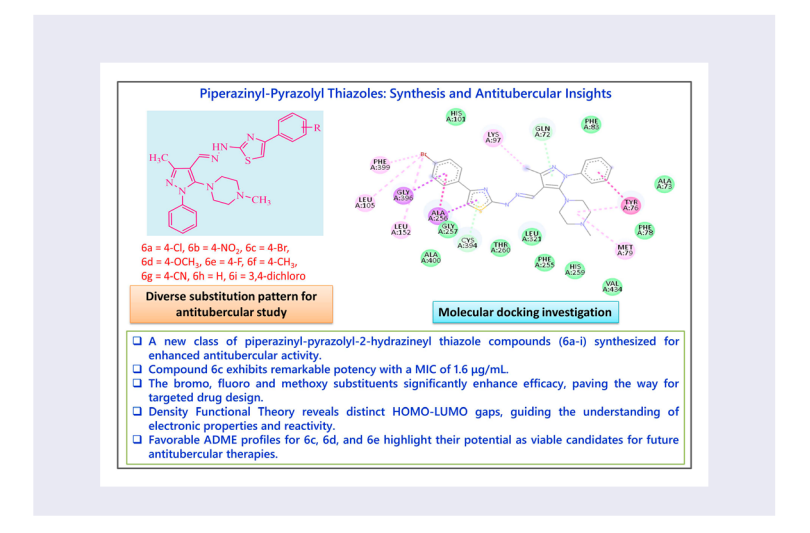
In the current research, a new series of piperazinyl-pyrazolyl-2-hydrazinyl thiazole derivatives (6a-6i) were synthesized and evaluated for their antitubercular activity against Mycobacterium tuberculosis H37Rv. The compounds were synthesized via a three-component reaction involving 3-methyl-5-(4methylpiperazin-1-yl)—1-phenyl-1H-pyrazole-4-carbaldehyde, thiosemicarbazide, and substituted phenacyl bromides (5a-5i) in ethanol under reflux conditions. The structures of the compounds were confirmed using ¹H NMR, ¹³C NMR, and FT-IR spectroscopy, which supported the successful formation of the thiazole core. The piperazinyl-pyrazolyl-2-hydrazinyl thiazole derivatives exhibited varying degrees of antitubercular activity, with compound 6c $(MIC = 1.6 \mu g/mL)$ showing the highest potency, comparable to the standard drugs isoniazid and ethambutol. The most active compounds follow the order as 6c (bromo substituent) > 6d (fluoro substituent) = **6e** (methoxy substituent) > **6a** (chloro substituent) = 6 g (nitrile substituent) with MIC ranging from (1.6–12.5 µg/mL). Other derivatives also displayed significant activity (MIC = $25-100 \,\mu\text{g/mL}$) in which the compound **6i** showed the lowest activity (MIC = 100 µg/mL). Molecular docking studies further supported its biological activity, revealing strong interactions with key residues of the target protein. The DFT analysis demonstrated that substituents such as bromine, methoxy, and fluorine affected the HOMO-LUMO energy gaps (3.89, 3.80, and 3.88 eV, respectively) and global softness $(0.517-0.526 \text{ eV}^{-1})$. ADME studies confirmed favorable pharmacokinetics for 6c, 6d, and 6e.

ARTICLE HISTORY

Received 5 December 2024 Accepted 27 January 2025

KEYWORDS

Piperazinyl-pyrazolyl-2hydrazinyl thiazole; antitubercular activity; Mycobacterium tuberculosis; structure—activity relationship; molecular docking; ADME; drug development



1. Introduction

Tuberculosis (TB) continues to be one of the biggest threats to world health [1, 2]. Mycobacterium tuberculosis (Mtb), the causative agent, mostly affects the lungs but can also infiltrate other organs, resulting in a substantial amount of disease and mortality on a global scale [3, 4]. Treatment attempts have been challenged by the growth of multidrug-resistant (MDR) and extensively drug-resistant (XDR) strains of Mtb, despite the availability of anti-tubercular medications [5, 6]. New anti-tubercular drugs with unique modes of action that can successfully fight resistant strains are thus desperately needed [7, 8]. Because of their various pharmacological characteristics, including anti-tubercular activity, heterocyclic compounds-especially those with thiazole and pyrazole moieties – have been the subject of promising research in recent years [9–12]. Thiazole derivatives are simple to synthesized and have numerous applications [13–16]. Derivatives of thiazoles are widely recognized for their diverse biological actions, which encompass anti-Alzheimer agents, anticancer, antiviral, antibacterial, anti-inflammatory, and antidermatophytic characteristics [17–26].

Thiazole compounds are highly significant structural motifs found in numerous physiologically active compounds, known for their ability to interact effectively with various biological targets. This makes thiazole an invaluable scaffold in drug discovery, particularly for developing novel therapeutics [27, 28]. Similarly, pyrazole derivatives have been extensively studied for their medicinal applications, with proven efficacy in antibacterial, anti-inflammatory, and anticancer agents [29, 30]. Combining thiazole and pyrazole moieties into a single molecular framework offers the potential to harness the unique pharmacological properties of each, resulting in a synergistic effect that enhances biological activity. This approach is particularly promising in the development of new antitubercular agents, as the fusion of these two heterocyclic cores may improve interactions with biological targets, optimize pharmacokinetic properties, and overcome drug resistance. Such a combination provides a versatile platform for exploring novel chemical entities with significant therapeutic potential against Mycobacterium tuberculosis.

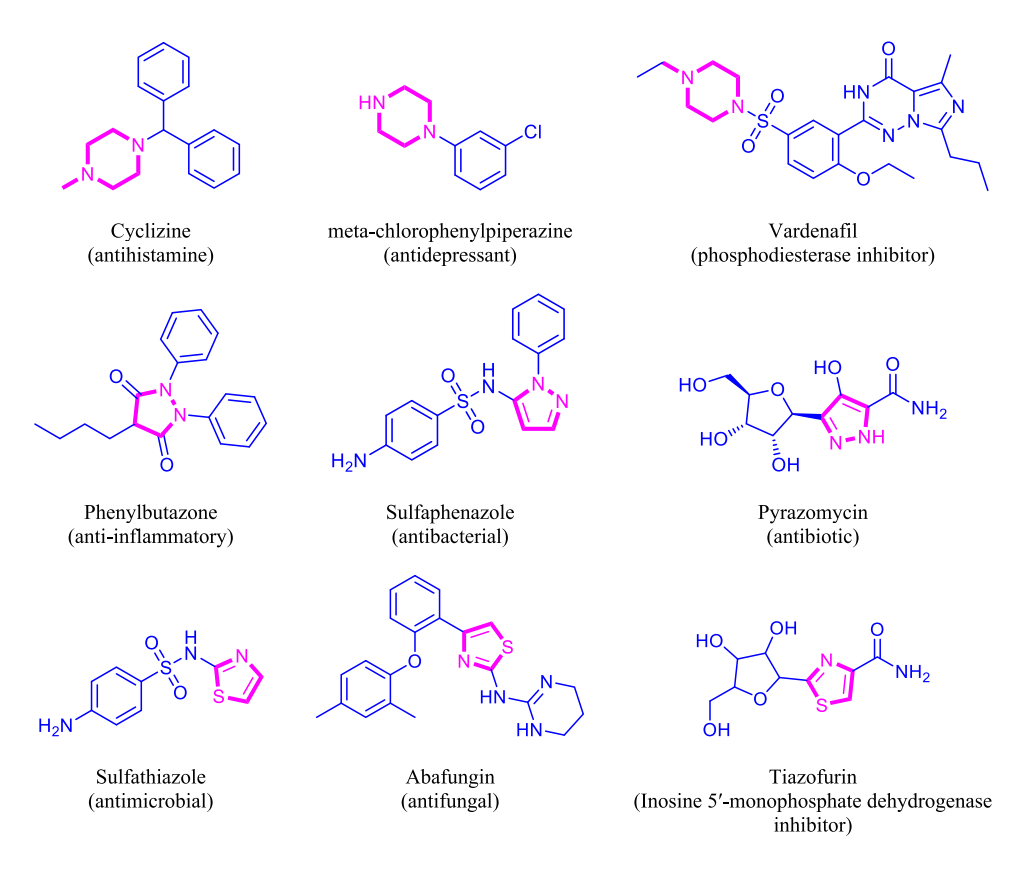


Figure 1. Some important heterocyclic compounds containing pyrazole, thiazole and piperazine ring structures.

The combined use of thiazole and pyrazole derivatives in the synthesis of piperazinyl-pyrazolyl-2-hydrazinyl thiazole compounds as effective anti-tubercular drugs is still not well covered in the literature, despite the substantial study on these compounds. Numerous heterocyclic derivatives containing pyrazoles and thiazoles, have been shown in earlier research to have antitubercular properties [31–34]. By interfering with important metabolic pathways like mycolic acid production, which is necessary for the bacterial cell wall, thiazole compounds, for instance, have been shown to have strong inhibitory effect against Mtb [35, 36]. The Figure 1 depicts some important heterocyclic compounds containing pyrazole, thiazole and piperazine ring structures. The objective of this study is to fill this vacuum by creating a novel class of piperazinyl-pyrazolyl-2-hydrazinyl thiazole derivatives and assessing their antitubercular efficacy through computational and experimental methods.

The current work focuses on using a three-component condensation process to synthesize a novel series of thiazole derivatives (**6a-6i**). This strategy is based on the concept that combining the pharmacophores of piperazine, pyrazole, and thiazole into a single molecule could improve the anti-tubercular activity of the resulting compounds. The pharmacokinetic properties of pharmacological molecules, specifically their solubility and bioavailability, are known to be enhanced by piperazine. The experimental evaluation of

the synthesized compounds against the Mtb H37Rv strain revealed promising results. Furthermore, molecular docking studies revealed the binding interactions of the synthesized compounds with the active sites of potential protein targets in Mtb, shedding light on the mechanisms underlying their antitubercular activity. This combined approach of synthetic chemistry and computational modeling strengthens the study's relevance, offering a more comprehensive foundation for the development of new therapeutic agents.

2. Materials and methods

2.1. General remarks

The chemicals used in the present research were purchased from Virion Enterprises, Mumbai. Thin layer chromatography (TLC) technique was used to track the completion of the reactions using Merck TLC Plates with Silica Gel 60 F_{254} . The FT-IR analysis was performed on Bruker FT-IR spectrophotometer (RAP analytical, Nashik). The NMR study was done using Bruker Advance 500 MHz NMR instrument (CIF, SPPU, Pune).

2.2. Experimental procedure for the synthesis of 3-methyl-5-(4-methylpiperazin-1-yl)—1-phenyl-1H-pyrazole-4-carbaldehyde

To synthesize compound 2, compound 1 (0.1 mol) was dissolved in dry dimethylformamide (DMF, 0.3 mol) in a reaction flask. Phosphorus oxychloride (POCl₃, 0.7 mol) was added dropwise to the reaction mixture under continuous stirring at room temperature. The reaction mixture was then heated to reflux ensuring the reaction proceeded to completion, as monitored by TLC. After completion, the reaction mixture was cooled to room temperature and poured into crushed ice, which caused the product to precipitate. The resulting solid was collected by filtration, washed thoroughly with cold water, and recrystallized using ethanol to obtain vompound 2 in its pure form. For the synthesis of compound 3, compound 2 (0.05 mol) was dissolved in dry DMF (50 mL) in a reaction flask, and potassium carbonate (K₂CO₃, 0.06 mmol) was added as a base to the solution. 1-Methylpiperazine (0.06 mmol) was then added gradually to the mixture under stirring. The reaction mixture was heated at 80-100°C for 4 h, with the progress of the reaction monitored by TLC. After completion, the reaction mixture was cooled to room temperature and poured into water, leading to the precipitation of the product. The precipitate was collected by filtration, washed with water, and purified by recrystallization to afford compound 3 in pure form (Scheme 1).

2.3. Experimental procedure for the synthesis of piperazinyl-pyrazolyl-2-hydrazinyl thiazole derivatives

The hydrazinyl thiazole derivatives were synthesized by reacting 3-methyl-5-(4-methylpiperazin-1-yl)—1-phenyl-1*H*-pyrazole-4-carbaldehyde (**3**, 5 mmol), thiosemicarbazide (**4**, 5 mmol), and substituted or unsubstituted phenacyl bromides (**5**, 5 mmol) in 10 mL of ethanol with 0.1 mL of glacial acetic acid as a catalyst (Scheme 2). Initially, 3-methyl-5-(4-methylpiperazin-1-yl)—1-phenyl-1*H*-pyrazole-4-carbaldehyde and thiosemicarbazide were dissolved in ethanol, followed by the addition of the 2-3 drops

of acetic acid. The mixture was stirred at room temperature for 5 min before heating the mixture to 80 °C in an oil bath. The reaction was maintained at this temperature for 50 min under reflux, with progress monitored by thin-layer chromatography (TLC). Following this, the appropriate phenacyl bromide (5a-5i) was added to the mixture under continuous stirring, Upon completion, the mixture was cooled to room temperature and then filtered, washed with cold ethanol, and dried. The structures were confirmed using ¹H NMR, ¹³C NMR, and IR spectroscopy. Table 1 depicts the physicochemical data of the synthesized piperazinyl-pyrazolyl-2-hydrazinyl thiazole derivatives (6a-6i).

2.4. Spectral data

2.4.1. (E)—4-(4-chlorophenyl)—2-(2-((3-methyl-5-(4-methylpiperazin-1-yl)—1-phenyl-1H-pyrazol-4-yl)methylene)hydrazinyl)thiazole (6a)

FT-IR (cm⁻¹): 3312, 3166, 3048, 2889, 2809, 1564, 1491, 1421, 1289, 1129, 1090, 980, 915, 915, 834, 754, 696, 649; ¹H NMR (500 MHz, DMSO- d_6) δ : 11.91 (s, 1H), 8.19 (s, 1H), 7.88 (d, I = 8.5 Hz, 2H), 7.61 (d, I = 8.5 Hz, 2H), 7.55 (t, I = 7.8 Hz, 2H), 7.49–7.42 (m, 3H), 7.36 (s, 1H), 3.44 (m, 4H), 3.29 (m, 4H), 2.85 (s, 3H), 2.38 (s, 3H); ¹³C NMR (126 MHz, DMSO- d_6) δ : 169.0, 149.8, 147.5, 147.0, 139.4, 136.0, 134.1, 132.3, 129.7, 129.1, 128.1, 127.7, 124.8, 108.5, 104.5, 53.3, 47.8, 42.9, 15.4.

2.4.2. (E)—2-(2-((3-methyl-5-(4-methylpiperazin-1-yl)—1-phenyl-1H-pyrazol-4yl)methylene)hydrazinyl)—4-(4-nitrophenyl)thiazole (6b)

FT-IR (cm⁻¹): 3318, 3140, 3071, 2991, 2890, 1573, 1501, 1423, 1327, 1174, 1114, 1045, 975, 920, 848, 754, 700, 655; ¹H NMR (500 MHz, DMSO- d_6) δ 12.02 (s, 1H), 8.28 (d, J = 8.9 Hz, 2H), 8.21 (s, 1H), 8.12 (d, J = 8.9 Hz, 2H), 7.70 (s, 1H), 7.61 (d, J = 7.3 Hz, 2H), 7.55 (t, $J = 7.8 \,\mathrm{Hz}$, 2H), 7.44 (t, $J = 7.3 \,\mathrm{Hz}$, 1H), 3.44–3.33 (m, 4H), 3.25 (m, 4H), 2.84 (s, 3H), 2.39 (s, 3H); 13 C NMR (126 MHz, DMSO- d_6) δ : 169.2, 149.1, 147.5, 147.1, 146.6, 141.2, 139.4, 136.4, 129.7, 128.1, 126.8, 124.8, 124.6, 108.6, 108.4, 53.3, 47.8, 42.9, 15.4.

2.4.3. (E)-4-(4-bromophenyl)-2-(2-((3-methyl-5-(4-methylpiperazin-1-yl)-1phenyl-1H-pyrazol-4-yl)methylene)hydrazinyl)thiazole (6c)

FT-IR (cm⁻¹): 3300, 3232, 3082, 3041, 2910, 2824, 1564, 1490, 1419, 1285, 1193, 1125, 1054, 1008, 916, 836, 748, 688, 652; 1 H NMR (500 MHz, DMSO- d_6) δ : 11.90 (s. 1H), 8.18 (s, 1H), 7.81 (d, J = 8.5 Hz, 2H), 7.60 (m, 4H), 7.55 (t, J = 7.8 Hz, 2H), 7.44 (t, J = 7.3 Hz, 2H), 7.81 (d, J = 8.5 Hz1H), 7.37 (s, 1H), 3.40 (s, 4H), 3.28 (s, 4H), 2.84 (s, 3H), 2.38 (s, 3H); ¹³C NMR (126 MHz, DMSO- d_6) δ : 169.0, 149.9, 147.5, 147.0, 139.4, 136.0, 134.4, 132.0, 129.7, 128.1, 128.0, 124.8, 120.9, 108.5, 104.6, 53.3, 47.8, 42.9, 15.4.

2.4.4. (E)-4-(4-methoxyphenyl)-2-(2-((3-methyl-5-(4-methylpiperazin-1-yl)-1phenyl-1H-pyrazol-4-yl)methylene)hydrazinyl)thiazole (6d)

FT-IR (cm⁻¹): 3375, 3132, 3080, 3022, 2983, 2882, 2827, 1560, 1491, 1423, 1296, 1244, 1177, 1119, 1025, 979, 918, 844, 755, 701; 1 H NMR (500 MHz, DMSO- d_6) δ : 11.85 (s, 1H), 8.18 (s, 1H), 7.79 (d, J = 8.7 Hz, 2H), 7.61 (d, J = 7.4 Hz, 2H), 7.55 (t, J = 7.8 Hz, 2H), 7.44(t, I = 7.3 Hz, 1H), 7.11 (s. 1H), 6.97 (d. I = 8.9 Hz, 2H), 3.79 (s. 3H), 3.41 (m. 4H), 3.27(m, 4H), 2.38 (s, 3H); 13 C NMR (126 MHz, DMSO- d_6) δ : 168.7, 159.2, 151.0, 147.5, 146.9, 139.4, 135.7, 129.7, 128.1, 127.3, 124.8, 114.4, 108.6, 101.5, 55.6, 53.3, 47.8, 42.9, 15.4.

 Table 1. Synthesized piperazinyl-pyrazolyl-2-hydrazinyl thiazole derivatives (6a-6i).

Br O H ₃ C H _N S 96 292-25 Br O H ₃ C H _N S 96 292-25 Br O H ₃ C H _N S 85 266-26 Br O H ₃ C H _N S 85 266-26 Br O H ₃ C H _N S 85 266-26 Br O H ₃ C H _N S 85 266-26 Br O H ₃ C H _N S 85 266-26 Br O H ₃ C H _N S 89 278-27	Entry	Phenacyl bromide	Product	Yield (%)	M.P. (°C)
Br			H, HN N		
Br		Br	N' N		
Br H ₃ C N S 96 292-29 Br H ₃ C N S 96 292-29 H ₃	5a	Cl	N.	92	260–262
Br		Br	H ₃ C S		
Br H ₃ C H _N S 85 266-26 Br H ₃ C H _N S 85 266-26 Br H ₃ C H _N S 84 282-28 H ₃ C H _N S 89 278-27	5 b	NO_2	Ch ₃	96	292–294
Br		$p \sim 0$	H HN N		
Br H_3 C H_3		Br	N N		
Br	6c	Br	N	85	266–267
Br		Br	H ₃ C S		
Br HN S N CH ₃ See 89 278-27	6d			84	282–284
N/N CH ₃ Se 89 278-27		Br O	H HN—// IĬ		
			N' N		
	6e	F			278-279 continued)

Table 1. Continued.

Entry	Phenacyl bromide	Product	Yield (%)	M.P. (°C)
		Me		
		H ₃ C N S		
	Br	N g		
		N-CH ₃		
6f	Me		83	240–242
OI.		CN	03	240 242
		H HN N		
	Br O	H ₃ C N S		
		N N N CH ₃		
6g	CN		93	294–295
og .			73	254 255
		H ₃ C, H _{HN} S		
	• 0	N. S		
	Br	N −CH ₃		
6h			88	218–220
		CI		
		H HN CI		
	Br O	H ₃ C N S		
		N N CH ₃		
6i	Cl		84	268–270
VI			U* 1	200-270

$2.4.5. \ (E)-4-(4-fluorophenyl)-2-(2-((3-methyl-5-(4-methylpiperazin-1-yl)-1-phenyl-1+pyrazol-4-yl)methylene) hydrazinyl) thiazole (6e)$

FT-IR (cm⁻¹): 3401, 3077, 2987, 2899, 2840, 1581, 1489, 1443, 1362, 1320, 1278, 1217, 1137, 1057, 1020, 981, 910, 846, 806, 758, 713, 649; 1 H NMR (500 MHz, DMSO- d_6) δ : 11.92 (s, 1H), 8.23 (s, 1H), 7.89 (dd, J = 8.7, 5.6 Hz, 2H), 7.61 (d, J = 7.5 Hz, 2H), 7.54 (t, J = 7.8 Hz, 2H), 7.43 (t, J = 7.4 Hz, 1H), 7.24 (m, 3H), 3.43 (m, 4H), 3.28 (m, 4H), 2.79 (s, 3H), 2.39 (s, 3H); 13 C NMR (126 MHz, DMSO- d_6) δ : 169.0, 162.0 (d, J = 244.4 Hz), 150.0, 147.5, 147.1, 139.4, 136.0, 131.9, 129.7, 128.0 (d, J = 4.3 Hz), 127.9, 124.7, 115.9 (d, J = 21.5 Hz), 108.5, 103.3, 53.0, 47.6, 42.7, 15.5.

2.4.6. (E) — 2-(2-((3-methyl-5-(4-methylpiperazin-1-yl) — 1-phenyl-1H-pyrazol-4-yl)methylene)hydrazinyl) — 4-(p-tolyl)thiazole (6f)

FT-IR (cm⁻¹): 3338, 3152, 3060, 2893, 1579, 1489, 1436, 1366, 1314, 1133, 1056, 980, 906, 822, 752, 647; 1 H NMR (500 MHz, DMSO- d_{6}) δ : 11.86 (s, 1H), 8.17 (s, 1H), 7.74 (d, J = 7.9 Hz, 2H), 7.61 (d, J = 7.9 Hz, 2H), 7.54 (t, J = 7.7 Hz, 2H), 7.44 (t, J = 7.3 Hz, 1H), 7.21 (m, 3H), 3.40 (s, 4H), 3.28 (s, 4H), 2.84 (s, 3H), 2.38 (s, 3H), 2.32 (s, 3H); 13 C NMR (126 MHz, DMSO- d_{6}) δ : 168.8, 151.2, 147.5, 146.9, 139.4, 137.2, 135.8, 132.6, 129.7, 129.6, 128.1, 125.9, 124.8, 108.6, 102.7, 53.3, 47.8, 42.9, 21.3, 15.4.

2.4.7. (E) -4-(2-(2-((3-methyl-5-(4-methylpiperazin-1-yl)-1-phenyl-1H-pyrazol-4-yl)methylene)hydrazinyl)thiazol-4-yl)benzonitrile (6 g)

FT-IR (cm⁻¹): 3311, 3120, 3055, 2963, 2904, 2212, 1565, 1494, 1419, 1281, 1174, 1123, 1048, 976, 914, 839, 757, 696; 1 H NMR (500 MHz, DMSO- d_{6}) δ : 11.97 (s, 1H), 8.21 (s, 1H), 8.04 (d, J = 8.5 Hz, 2H), 7.87 (d, J = 8.5 Hz, 2H), 7.61 (m,, 3H), 7.55 (t, J = 7.9 Hz, 2H), 7.44 (t, J = 7.3 Hz, 1H), 3.33 (s, 4H), 3.28 (s, 4H), 2.81 (s, 3H), 2.38 (s, 3H); 13 C NMR (126 MHz, DMSO- d_{6}) δ : 169.1, 149.3, 147.5, 147.1, 139.4, 139.3, 136.3, 133.2, 129.7, 128.1, 126.6, 124.8, 119.5, 110.0, 108.4, 107.6, 53.3, 47.8, 42.9, 15.4.

2.4.8. (E)—2-(2-((3-methyl-5-(4-methylpiperazin-1-yl)—1-phenyl-1H-pyrazol-4-yl)methylene)hydrazinyl)—4-phenylthiazole (6 h)

FT-IR (cm⁻¹): 3341, 3075, 2958, 2908, 1581, 1493, 1438, 1365, 1286, 1137, 1051, 981, 910, 847, 814, 742, 655; 1 H NMR (500 MHz, DMSO- d_{6}) δ : 11.89 (s, 1H), 8.17 (s, 1H), 7.86 (d, J = 7.4 Hz, 2H), 7.61 (d, J = 7.6 Hz, 2H), 7.55 (t, J = 7.8 Hz, 2H), 7.46–7.39 (m, 3H), 7.33–7.26 (m, 2H), 3.48–3.34 (m, 4H), 3.31–3.25 (m, 4H), 2.84 (s, 3H), 2.38 (s, 3H); 13 C NMR (126 MHz, DMSO- d_{6}) δ : 168.8, 147.5, 146.9, 139.4, 135.8, 135.3, 129.7, 129.1, 128.1, 128.0, 126.0, 124.9, 108.6, 103.7, 53.3, 47.8, 42.9, 15.3.

2.4.9. (E)—4-(3,4-dichlorophenyl)—2-(2-((3-methyl-5-(4-methylpiperazin-1-yl)—1-phenyl-1H-pyrazol-4-yl)methylene)hydrazinyl)thiazole (6i)

FT-IR (cm⁻¹): 3320, 3010, 2893, 1553, 1413, 1288, 1127, 1051, 985, 912, 824, 749; ¹H NMR (500 MHz, DMSO- d_6) δ : 11.94 (s, 1H), 8.19 (s, 1H), 8.09 (d, J = 2.0 Hz, 1H), 7.85 (dd, J = 8.4, 2.0 Hz, 1H), 7.67 (d, J = 8.4 Hz, 1H), 7.61 (d, J = 7.4 Hz, 2H), 7.54 (m, 3H), 7.44 (t, J = 7.3 Hz, 1H), 3.43–3.34 (m, 4H), 3.28 (m, 4H), 2.84 (s, 3H), 2.38 (s, 3H); ¹³C NMR (126 MHz, DMSO- d_6) δ : 169.1, 149.3, 147.5, 147.1, 139.4, 139.3, 136.3, 133.2, 129.7, 128.1, 126.6, 125.4, 124.8, 119.5, 110.0, 108.4, 107.6, 53.3, 47.8, 42.9, 15.4.

2.5. Antitubercular screening

The antitubercular activity of the synthesized compounds was assessed using the microplate Alamar Blue assay (MABA) against *Mycobacterium tuberculosis* H37Rv strain (ATCC No. 27294). This method, which is non-toxic and employs a thermally stable reagent, provides a good correlation with the proportional and BACTEC radiometric methods. The procedure involved adding 200 μL of sterile deionized water to the outer perimeter wells of a sterile 96-well microplate to minimize evaporation. Wells with only the medium and Alamar Blue mixture were used as blanks to eliminate background interference in color development. Subsequently, 100 μL of Middlebrook 7H9 broth was added

to the inner wells, and serial dilutions of the test compounds were prepared directly on the plate, with final concentrations ranging from 100 µg/mL to 0.2 µg/mL. Plates were sealed with parafilm and incubated at 37°C for five days. After this period, 25 µLof a freshly prepared 1:1 mixture of Alamar Blue reagent and 10% Tween 80 were added to each well, followed by a 24-hour incubation. The results were determined by the color change in the wells: blue indicated no bacterial growth (i.e. effective inhibition by the compound), while pink indicated bacterial growth. The minimum inhibitory concentration (MIC) was defined as the lowest concentration that prevented the color change from blue to pink. Standard antitubercular drugs – isoniazid, ethambutol, pyrazinamide, rifampicin, and streptomycin - were used as positive controls, with MIC values of 1.6, 1.6, 3.125, 0.8, and 0.8 µg/mL, respectively, to validate the assay's accuracy. All experiments were performed in triplicate to ensure reproducibility and reliability of the results.

2.6. Molecular docking

The molecular docking study of the most active compounds 6c, 6d and 6e were evaluated to know the various binding interactions [37]. The steps are as follows-

Protein Preparation: The target protein, P45014 α -sterol demethylase (CYP51) with PDB ID: 1E9X, was downloaded from the Protein Data Bank (PDB). All heteroatoms (small molecules, ions, and water molecules) were removed to ensure that only the receptor protein remained for ligand interaction. If the protein contained multiple chains, they were split to ensure docking occurred only within the relevant binding site. The structure of the target protein, $P45014\alpha$ -sterol demethylase (CYP51), was validated to confirm structural integrity post-processing.

Ligand Preparation: Ligands were prepared in PDB format. If necessary, conversion to PDB format was performed. The size of the ligand was kept below 15 KB to maintain high accuracy and efficiency during docking, as larger ligands with more atoms and rotatable bonds can decrease AutoDock Vina's accuracy.

Cavity Detection: CB-Dock employs a blind docking approach, automatically identifying and analyzing potential binding cavities on the protein surface. The software detects putative binding sites, focusing on larger cavities where ligands are likely to bind. The top cavities were selected based on their size for further docking analysis. For this research, the default number of five cavities was used, although this can be adjusted if necessary.

Docking Procedure: Docking was conducted within the detected cavities, and parameters such as the center and size of the grid box were customized to ensure precise ligand placement. The docking was performed with a blind docking approach, considering all potential binding sites for unbiased analysis.

Reranking and Binding Pose Selection: Following the docking process, the docked poses were reranked according to their docking score, with the scoring function reflecting the predicted binding affinity between the protein and ligand. The conformation with the lowest docking score was considered the best binding pose, and the corresponding cavity was designated as the optimal binding site for the ligand.

Output and Analysis: The top binding conformation was visualized, and interactions such as hydrogen bonding, hydrophobic interactions, and pi-stacking with key residues of



CYP51 were analyzed to understand the molecular basis of binding affinity. Visualization tools ensured accurate assessment of molecular interactions contributing to ligand stability within the binding site.

2.7. DFT details

The DFT method using the B3LYP functional was used for the computational investigation [38, 39]. The Gaussian-03 Programme package was used to do DFT simulations without any geometry constraints on an Intel (R) Core (TM) i5 computer [40]. The geometry of the 6c, 6d, and 6e compounds was optimized in the gas phase using the DFT method, the B3LYP functional, and the 6-311G(d,p) basis set. The 6-311G(d,p) basis set, the B3LYP functional, and the TD-DFT method were used to compute the HOMO and LUMO. The molecular visualization application Gauss View 4.1.2 was used to generate optimized geometry, MESP plot, HOMO, and LUMO images [41].

2.8. ADME study

SwissADME; a web-based software that provides free access was used for evaluating the pharmacokinetics, drug-likeness, and medicinal chemistry friendliness of the compounds [42].

3. Results and discussion

3.1. Chemistry

The thiazole derivatives (6a-6i) were synthesized by three component condensation of 3-methyl-5-(4-methylpiperazin-1-yl)-1-phenyl-1H-pyrazole-4-carbaldehyde (3), thiosemicarbazide (4), and substituted or unsubstituted phenacyl bromides (5a-5i) in ethanol using glacial acetic acid as a catalyst. The spectral data, including IR, ¹H NMR, and ¹³C NMR spectra were in full agreement with the structures of the synthesized thiazoles. The ¹H NMR spectra provided detailed information about the electronic environment of the protons and carbons within the molecules. The multiplicity of the proton signals and the coupling constants helped to confirm the substitution patterns on the phenyl rings, while the characteristic imine and thiazole carbon signals in the ¹³C NMR spectra were consistent with the expected structures [43-45]. The FT-IR spectra of the synthesized thiazole compounds (6a-6i) exhibit characteristic absorptions that confirm the presence of functional groups [46-48]. A strong peak around 3312-3401 cm⁻¹ in all compounds indicates N-H stretching from the hydrazinyl group, which is slightly shifted due to hydrogen bonding. For compound 6a, the peak at 3312 cm⁻¹ corresponds to the stretching vibration of the secondary amine (-NH) group, while **6b** shows a similar stretch at $3317 \, \text{cm}^{-1}$. The C–H stretching vibrations from aromatic rings are observed between $3040-3079 \text{ cm}^{-1}$, confirming the presence of phenyl groups. The peaks between 2881 and 2990 cm⁻¹ correspond to aliphatic C-H stretches in the methyl and piperazine groups. Notably, the carbonyl group is absent in these spectra, consistent with the structure. The C = N stretching of the thiazole ring appears as a sharp band around 1560–1579 cm⁻¹, confirming the

presence of the conjugated imine system. The nitro group in compound 6b exhibits a characteristic asymmetric stretch at 1572 cm⁻¹ and symmetric stretching at 1326 cm⁻¹, further validating the substitution on the aromatic ring. Peaks between 600 and 800 cm⁻¹ correspond to C-Cl, C-Br, and other halo-aromatics in compounds like **6a**, **6c**, and **6e**. The ¹H NMR spectra of compounds 6a-6i show clear signals corresponding to the proton environments, confirming their structures. The singlet at δ 11.85–12.0 in all compounds is assigned to the proton of the hydrazone N-H group, indicating strong deshielding due to its conjugation with the thiazole system. In **6a** and **6b**, the signals at δ 8.19–8.28 correspond to the C = N proton, while the doublets at δ 7.88–8.12 (J = 8.5 Hz for **6a**, J = 8.9Hz for **6b**) indicate ortho-protons of the aromatic rings. The protons of the piperazine ring resonate between δ 3.29 and 3.44 as multiplets, integrating for four protons each, confirming the aliphatic environment. For compound 6d, the methoxy group appears as a singlet at δ 3.79, indicating shielding of the protons due to electron-donating effects. The methyl protons of the pyrazole and piperazine groups appear as singlets around δ 2.38–2.85, showing consistent chemical shifts across all derivatives. Coupling constants, especially in 6a-6f, support ortho - and meta-coupling interactions within the aromatic rings, with values around 7.3–8.5 Hz, confirming the substitution patterns. The ¹³C NMR spectra of compounds 6a-6i display distinct signals for the carbon atoms, consistent with their structures. In all compounds, the signals around δ 168–169 correspond to the imine carbon (C = N), indicating significant deshielding due to its conjugation with the thiazole ring. For compound 6b, the nitro group causes a downfield shift in the aromatic carbons at δ 129–141 ppm. The carbon atoms of the pyrazole ring resonate around δ 147–150, while the thiazole carbons are observed between δ 136 and 139 in all compounds. The methoxysubstituted compound **6d** shows a characteristic signal at δ 55.61, indicating the presence of the – OCH₃ group. In contrast, the methyl carbons in compounds **6a-6i** appear as singlets around δ 15.37–15.52 ppm, confirming their aliphatic nature. The carbon signals for the piperazine ring carbons are located between δ 42 and 53, further validating the structure. The fluorine-substituted aromatic ring in compound 6e exhibits a distinct coupling with carbon at δ 162.0 (J = 244.4 Hz), reflecting significant deshielding caused by the highly electronegative fluorine atom.

3.2. Antitubercular study

The anti-tubercular activity of synthesized thiazole derivatives was evaluated against Mycobacterium tuberculosis (H37Rv strain) using the microplate Alamar Blue assay (MABA), revealing a range of minimum inhibitory concentration (MIC) values, which indicated varying levels of potency (Table 2). Among the tested compounds, 6c emerged as the most potent with an MIC of 1.6 µg/mL, which matches the standard drugs isoniazid and ethambutol. The bromophenyl substitution on the thiazole ring in **6c** likely contributes to this enhanced activity, suggesting that electron-withdrawing groups, such as bromine, play a significant role in boosting anti-tubercular potency. Compounds **6d** and **6e**, both of which demonstrated an MIC of 3.125 µg/mL, displayed anti-tubercular activity comparable to pyrazinamide, another standard drug, indicating that methoxyphenyl and fluorophenyl substituents also confer substantial efficacy against M. tuberculosis. In contrast, 6i exhibited the weakest activity with an MIC of 100 µg/mL, suggesting that the dichlorophenyl substitution diminishes efficacy, possibly due to steric or electronic factors. Other compounds,

Table 2. Anti-Mycobacterial activity of the synthesized thiazole derivatives against *M. tuberculosis*.

Entry	Names of the compounds	MIC (μg/mL)
6a	(E)—4-(4-chlorophenyl)—2-(2-((3-methyl-5-(4-methylpiperazin-1-yl)—1-phenyl-1H-pyrazol-4-yl)methylene)hydrazinyl)thiazole	12.5
6b	(E)—2-(2-((3-methyl-5-(4-methylpiperazin-1-yl)—1-phenyl-1 <i>H</i> -pyrazol-4-yl)methylene)hydrazinyl)—4-(4-nitrophenyl)thiazole	50
6c	(E)—4-(4-bromophenyl)—2-(2-((3-methyl-5-(4-methylpiperazin-1-yl)—1-phenyl-1H-pyrazol-4-yl)methylene)hydrazinyl)thiazole	1.6
6d	(E)—4-(4-methoxyphenyl)—2-(2-((3-methyl-5-(4-methylpiperazin-1-yl)—1-phenyl-1 <i>H</i> -pyrazol-4-yl)methylene)hydrazinyl)thiazole	3.125
6e	(E)—4-(4-fluorophenyl)—2-(2-((3-methyl-5-(4-methylpiperazin-1-yl)—1-phenyl-1 <i>H</i> -pyrazol-4-yl)methylene)hydrazinyl)thiazole	3.125
6f	(F)—2-(2-((3-methyl-5-(4-methylpiperazin-1-yl)—1-phenyl-1 <i>H</i> -pyrazol-4-yl)methylene)hydrazinyl)—4-(<i>p</i> -tolyl)thiazole	25
6g	(F)—4-(2-(2-((3-methyl-5-(4-methylpiperazin-1-yl)—1-phenyl-1H-pyrazol-4-yl)methylene)hydrazinyl)thiazol-4-yl)benzonitrile	12.5
6h	(F)—2-(2-((3-methyl-5-(4-methylpiperazin-1-yl)—1-phenyl-1 <i>H</i> -pyrazol-4-yl)methylene)hydrazinyl)—4-phenylthiazole	50
6i	(E)—4-(3,4-dichlorophenyl)—2-(2-((3-methyl-5-(4-methylpiperazin-1-yl)—1-phenyl-1 <i>H</i> -pyrazol-4-yl)methylene)hydrazinyl)thiazole	100
Standards	Isoniazid	1.6
	Ethambutol	1.6
	Pyrazinamide	3.125
	Rifampicin	0.8
	Streptomycin	0.8

such as 6a and 6 g, with MIC values of 12.5 µg/mL, displayed moderate anti-tubercular activity, indicating that the chlorophenyl and benzonitrile groups contribute to the activity, although not as strongly as bromophenyl or methoxyphenyl substitutions. Compounds 6b and 6 h, both with MIC values of 50 µg/mL, showed relatively lower efficacy, suggesting that the nitrophenyl and phenyl groups are less favorable for anti-mycobacterial activity. This variation in potency among the derivatives highlights a clear structure-activity relationship (SAR), where electron-withdrawing groups such as bromine improve efficacy, while bulkier or electron-donating groups, like nitrophenyl and dichlorophenyl, reduce activity [46]. When compared to standard anti-tubercular drugs, rifampicin and streptomycin, which both had an MIC of 0.8 μg/mL, remain the most potent. Isoniazid and ethambutol, with an MIC of 1.6 µg/mL, exhibited potency equivalent to 6c, while pyrazinamide (MIC = $3.125 \,\mu g/mL$) displayed similar efficacy to **6d** and **6e**. Overall, this study identifies several thiazole derivatives with significant anti-tubercular potential, particularly 6c, which demonstrated activity equivalent to the key standard drugs. Bromine, as an electronwithdrawing substituent, enhances antitubercular activity by increasing the compound's lipophilicity, enabling better penetration through the lipid-rich mycobacterial cell wall. It also contributes to stabilizing interactions with the target protein through hydrogen and halogen bonding. The findings suggest that further structural optimization and in vivo testing could lead to the development of novel therapeutic agents, with the bromophenyl group being a key factor in enhancing anti-tubercular efficacy.

3.3. DFT study

The optimized structures of compounds **6c**, **6d**, and **6e** (Figure 2) show distinct spatial arrangements influenced by their respective substituents. All compounds possess a

thiazole ring at the core, attached to the pyrazole moiety, forming a rigid and planar framework. The phenyl groups attached to the thiazole ring exhibit varying degrees of distortion depending on the nature of the substituent (bromo, methoxy, or fluoro). In 6c, the bromo group on the phenyl ring adds electron-withdrawing properties, slightly pulling electron density from the ring. In contrast, the methoxy group in 6d is an electron-donating substituent, potentially affecting the electronic distribution and interactions with biological targets. The fluoro group in 6e is smaller but also electron-withdrawing, affecting both lipophilicity and electron distribution. The planar structure enables potential π - π stacking interactions, which are crucial for antitubercular activity. Furthermore, the different MIC values (1.6 μg/mL for **6c** and 3.125 μg/mL for **6d** and **6e**) correlate with the variations in substituents. The stronger activity of 6c could be attributed to the bromo group enhancing interaction with the Mycobacterium tuberculosis enzyme active site, compared to the methoxy and fluoro groups in 6d and 6e.

The molecular electrostatic potential (MESP) plots of the compounds 6c, 6d, and 6e are depicted in Figure 3. The MESP plot of compound 6c reveals the electronic distribution, showing areas of electropositivity (blue) around the nitrogen and bromine atoms and areas of electronegativity (red) near the bromophenyl group [48]. This distribution suggests potential interactions with biological targets, particularly in regions of polar interaction. In comparison, 6d and 6e exhibit similar electrostatic trends, but with differences due to their methoxy and fluorine substituents, respectively. The methoxy group in 6d introduces an electron-donating effect, while the fluorine in 6e enhances electronegativity. These electronic differences influence the interaction with the active site of the target, impacting the compounds' antitubercular efficacy. Notably, compound 6c has the lowest MIC value (1.6 µg/mL), likely due to the favorable electrostatic profile, indicating stronger interaction with biological targets compared to 6d and 6e, which have higher MIC values $(3.125 \mu g/mL)$.

The HOMO and LUMO are very important properties to understand electronic characteristics [49-51]. The HOMO and LUMO distributions in the given molecular structures (Figure 4) show distinct localization patterns across the compounds. In compound 6c, the electron-withdrawing bromine localizes the HOMO over the brominated phenyl and thiazole rings, while the LUMO is mainly distributed over the hydrazine and thiazole ring, indicating a clear pathway for electronic transitions. In comparison, compound 6d, which contains an electron-donating methoxy group, exhibits enhanced electron density in the HOMO across the phenyl and pyrazole rings. Meanwhile, the LUMO is concentrated on the thiazole and pyrazole parts, which reflects the electron-donating influence of the methoxy group. In compound 6e, the highly electronegative fluorine causes the HOMO to concentrate more on the thiazole and pyrazole rings, with less localization on the fluorinated phenyl ring, while the LUMO extends from the thiazole to the fluorinated phenyl ring. This shows that fluorine's electron-withdrawing nature shifts the electronic density, altering the regions of HOMO and LUMO distribution compared to the other compounds. Table 3 contains the electronic and global reactivity parameters of compounds 6c, 6d and 6e. The HOMO-LUMO values of compounds 6c, 6d, and 6e reflect the influence of their substituents on electronic properties. Compound 6c (bromophenyl) has the largest energy gap (3.89 eV), due to the electron-withdrawing nature of bromine, suggesting lower reactivity. Compound 6d (methoxyphenyl) shows the smallest gap (3.80 eV), as the electron-donating methoxy group enhances reactivity. Compound **6e** (fluorophenyl)

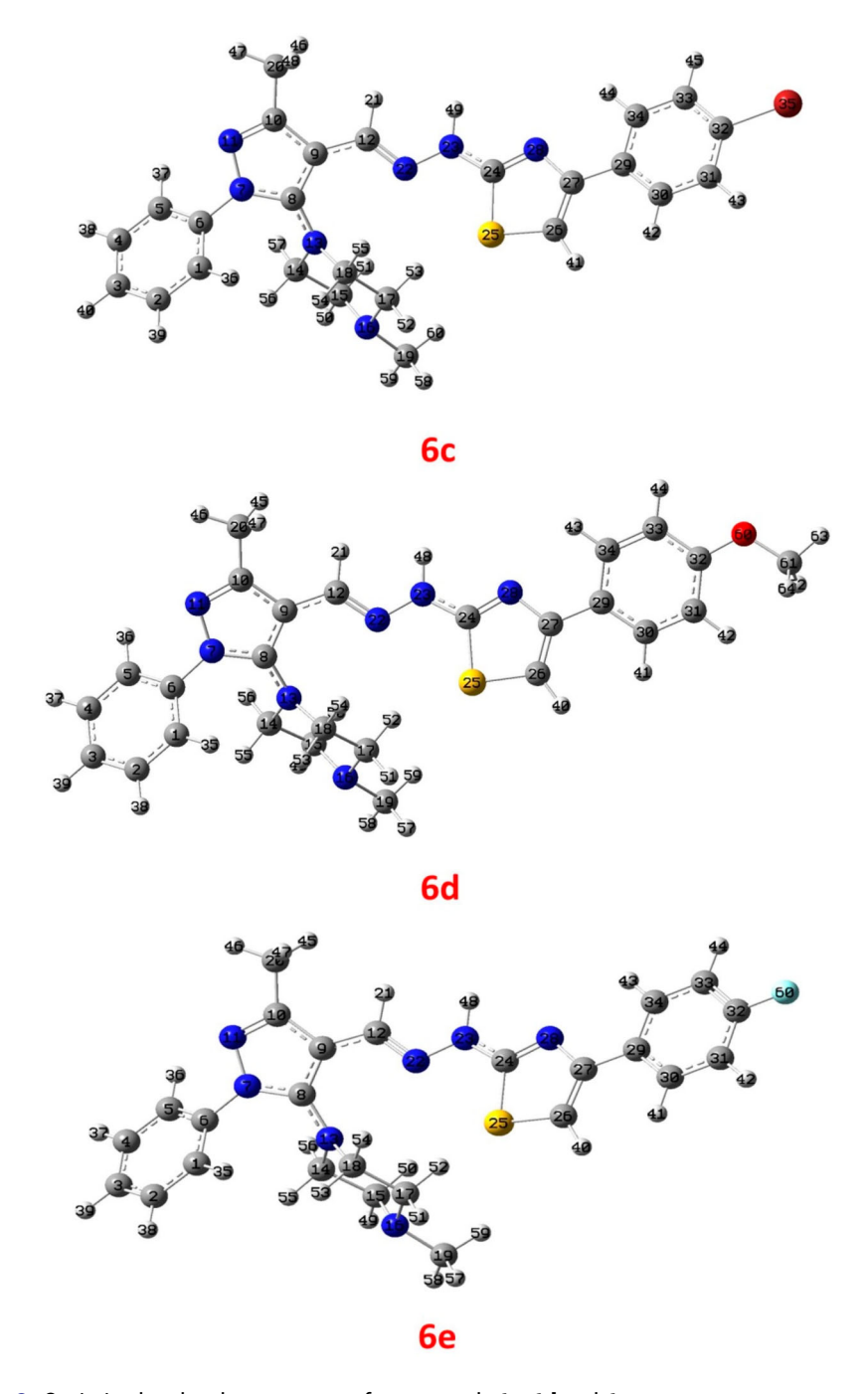


Figure 2. Optimized molecular structures of compounds 6c, 6d and 6e.

has an intermediate gap (3.88 eV), with fluorine's electronegativity stabilizing the structure. The comparative analysis of the global descriptor parameters reveals the influence of the different substituents (bromine, methoxy, and fluorine) on the electronic properties of

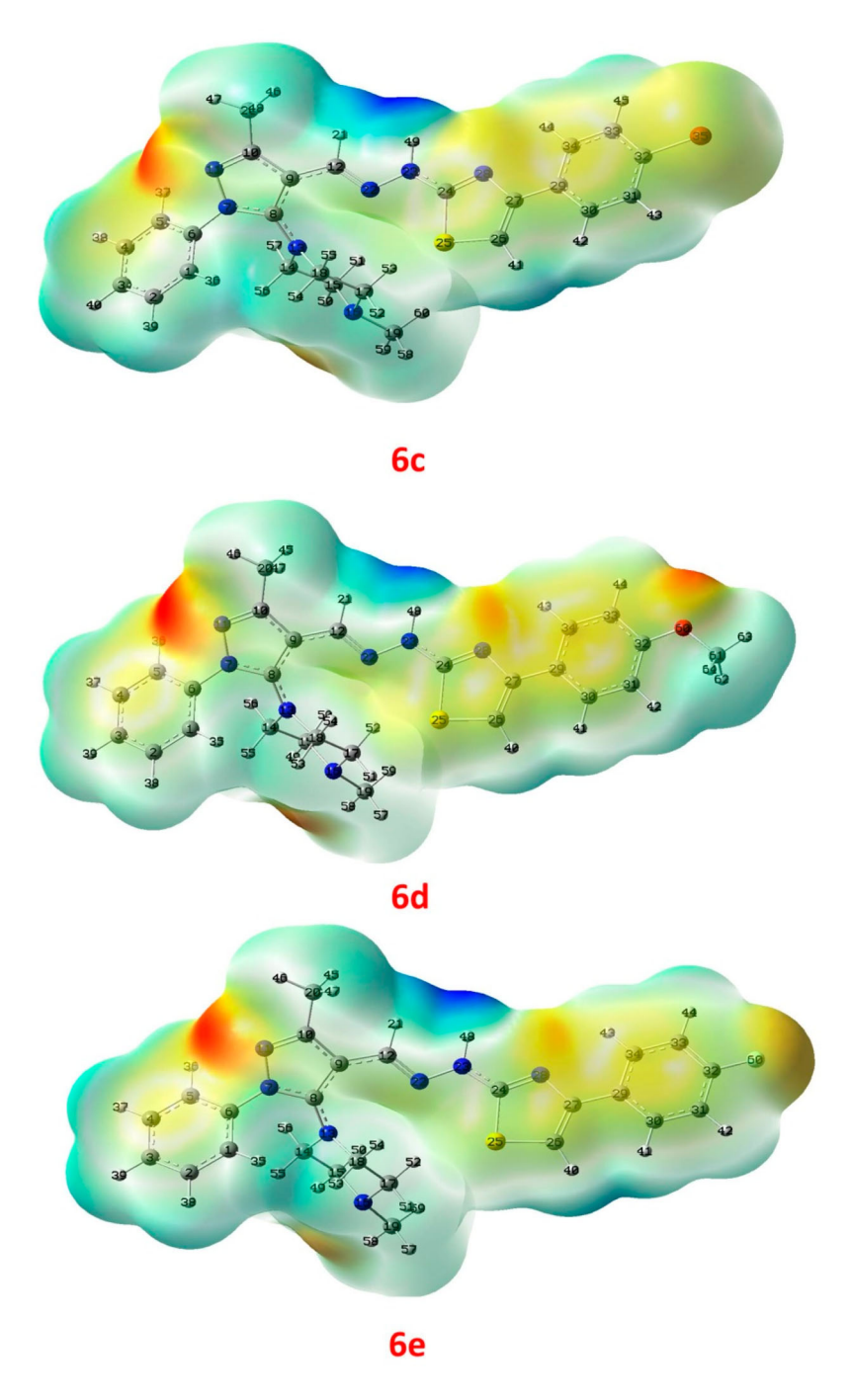


Figure 3. Molecular electrostatic surface potential plots of compounds 6c, 6d and 6e.

compounds **6c**, **6d**, and **6e**. Compound **6c**, with a bromine substituent, shows the highest ionization potential (5.34 eV) and chemical potential (-3.395 eV), indicating a lower ability to donate electrons compared to the other compounds. The higher electrophilicity

Table 3. The electronic and global reactivity parameters of compounds **6c**, **6d** and **6e**.

Compound	E _{HOMO} (eV)	E _{LUMO} (eV)	Eg (eV)	χ (eV)	I (eV)	A (eV)	μ (eV)	η (eV)	S (eV ⁻¹)	ω (eV)	Δ Nmax
6c	-5.34	-1.45	3.89	3.395	5.34	1.45	-3.395	1.945	0.514	2.963	1.746
6d	-5.08	-1.28	3.80	3.180	5.08	1.28	-3.180	1.900	0.526	2.661	1.674
6e	-5.27	-1.39	3.88	3.330	5.27	1.39	-3.330	1.940	0.515	2.858	1.716

Where, E_{HOMO}: Highest Occupied Molecular Orbital energy, E_{LUMO} Lowest Unoccupied Molecular Orbital energy, Eg: Energy gap, χ : Electronegativity, **1**: Ionization Potential, **A**: Electron Affinity, μ : Chemical Potential, η : Chemical Hardness, **S**: Global Softness, ω: Electrophilicity Index, Maximum Electron Transferred

index for 6c suggests it is more reactive toward electrophiles. In contrast, compound 6d, with a methoxy group, has the lowest ionization potential (5.08 eV) and electronegativity (3.180 eV), reflecting its greater electron-donating capability. The methoxy group increases electron density, resulting in the highest global softness (0.526 eV⁻¹), making 6d the most chemically reactive among the three compounds. Compound 6e, with a fluorine substituent, falls between the other two in terms of ionization potential and chemical potential, showing a balance between electron-withdrawing and donating effects. The fluorine's electronegativity slightly decreases its softness $(0.515 \,\mathrm{eV}^{-1})$, but its electrophilicity index ($\omega = 2.858 \, \text{eV}$) remains high, indicating significant reactivity. Thus, the substituents strongly influence electron distribution and reactivity, with bromine and fluorine being more electron-withdrawing and methoxy being electron-donating. Correlation of electronic properties and biological properties has been important criterion [52]. The antitubercular activity (MIC) shows a correlation with the band gap (Eg), as compound **6c** with the highest activity (MIC = $1.6 \mu g/mL$) has the largest band gap (Eg = 3.89 eV). Compounds **6d** and **6e**, with lower activity (MIC = $3.125 \,\mu\text{g/mL}$), have slightly smaller band gaps. This suggests that a larger band gap may favor antitubercular activity, though other factors might also contribute.

3.4. Molecular docking analysis

The molecular docking study of compounds 6c, 6d, and 6e was performed to evaluate their binding interactions (Figures 5–7) with the target protein P45014 α -sterol demethylase (CYP51, PDB ID: 1E9X). Protein preparation involved removing all heteroatoms and separating chains for proper docking. Ligands were prepared in PDB format, ensuring the size was below 15 KB for accuracy in AutoDock Vina. CB-Dock identified five potential binding cavities on the protein surface, where the ligands were docked based on cavity size and location. The docked poses were prioritized based on binding affinity, where the lowest docking score identified the most favorable binding site. The top conformations were then examined for important interactions, such as hydrogen bonds, hydrophobic interactions, and pi-stacking. The docking interaction of compound 6c with its target protein shows a variety of stabilizing interactions. Notably, pi-pi stacking interactions are formed with Tyr A:76 and Phe A:78, stabilizing the aromatic rings of the ligand, which is crucial for its proper orientation within the binding site. Additionally, pi-alkyl interactions with Leu A:152, Leu A:105, and Phe A:399 contribute to hydrophobic stabilization, particularly with the phenyl and benzene rings of the compound. Key hydrogen bonds between the ligand and Gly A:257 and Ala A:256 enhance binding affinity by anchoring the ligand to the protein. The ligand also benefits from van der Waals interactions with residues like Gly

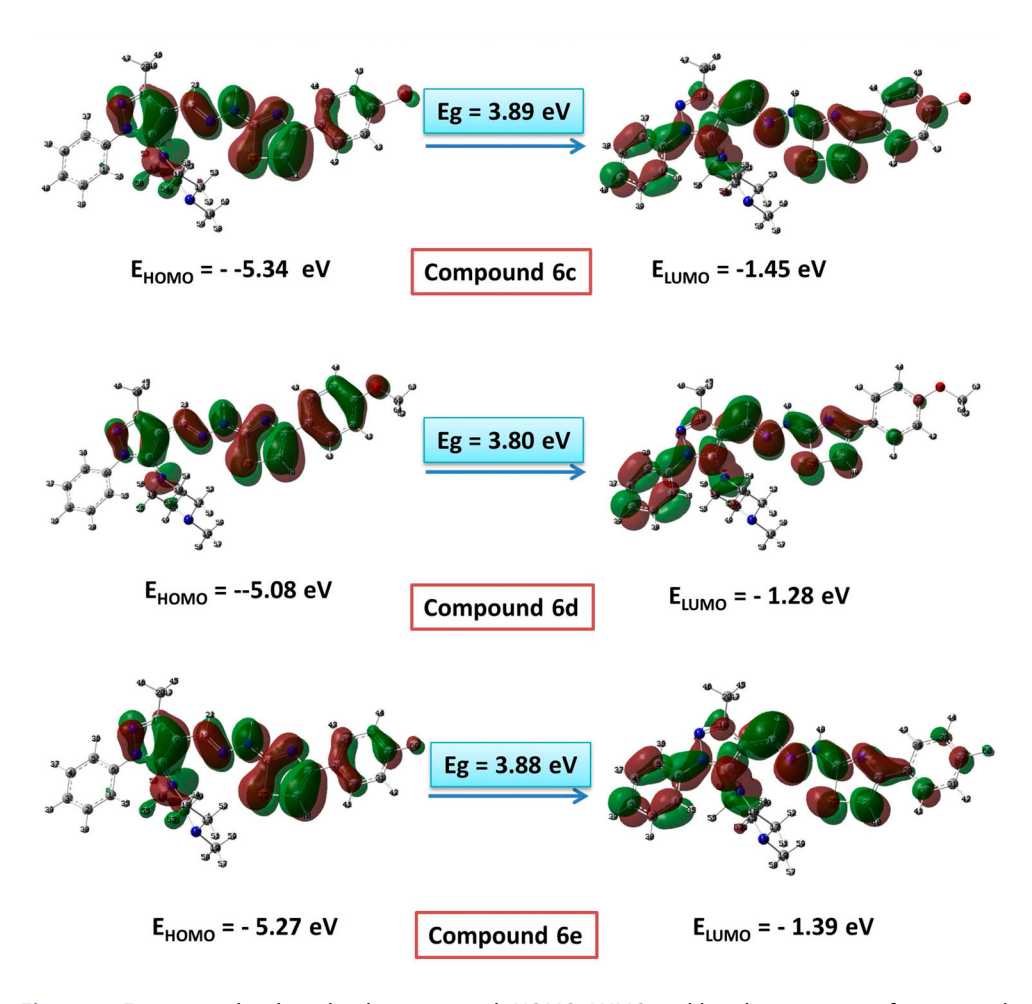


Figure 4. Frontier molecular orbital pictures with HOMO, LUMO and band gap energy of compounds **6c**, **6d** and **6e**.

A:396, Ala A:400, Leu A:321, and His A:259, which provide general stabilization within the binding pocket. Moreover, pi-sigma interactions with Phe A:255 and Phe A:399 further support the non-covalent stabilization of the ligand. Collectively, these interactions – hydrophobic, pi-stacking, hydrogen bonding, and van der Waals – suggest that compound **6c** binds strongly and stably within the protein's active site, making it a promising candidate for biological activity. The docking interaction image of compound **6d** reveals various non-covalent interactions with the protein target. Pi-pi stacking interactions (pink) are observed between the ligand and Phe A:83, Tyr A:76, and Met A:79, stabilizing the aromatic rings within the binding pocket. Pi-alkyl interactions (light purple) with Arg A:96, Phe A:83, and Met A:79 further strengthen the ligand's hydrophobic binding. Notable van der Waals interactions (light green) involve residues like Val A:87, Val A:88, Ser A:252, and Leu A:100, providing additional stability and fitting the ligand within the active site. Hydrogen bonds, although not explicitly highlighted in this visualization, are typically critical for binding, and may also be present to anchor specific portions of the ligand. The diverse

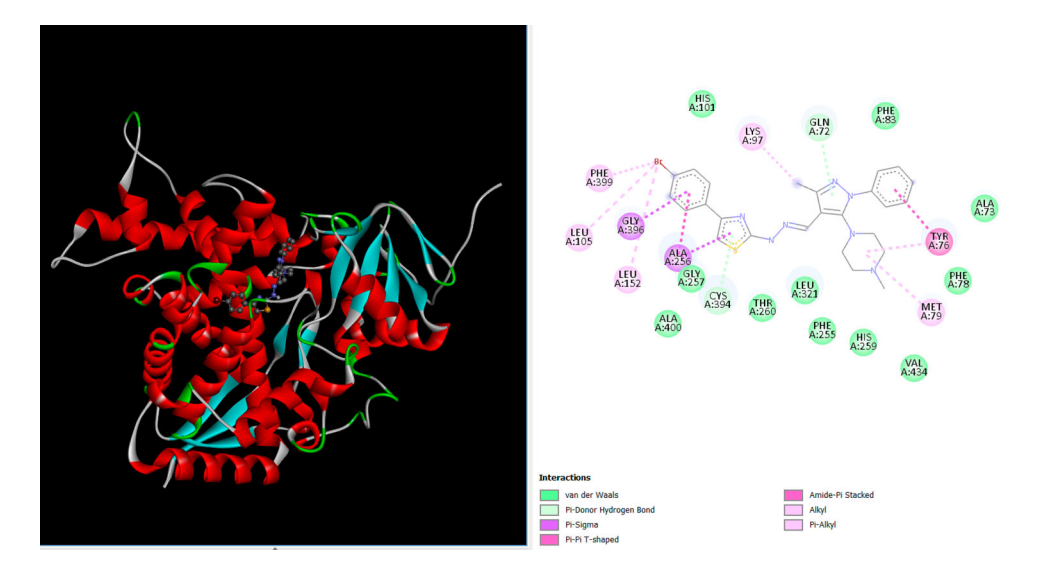


Figure 5. 3D and 2D interactions of compound 6c with target.

interactions, including pi-stacking, alkyl interactions, and van der Waals forces, indicate that compound 6d has a strong affinity for the protein target, occupying the binding site with both hydrophobic and aromatic stabilization mechanisms. These interactions suggest that the compound can potentially exhibit strong biological activity by effectively binding to the target protein. The docking interaction image of compound **6e** reveals a rich array of non-covalent interactions between the ligand and its protein target, contributing to a stable binding pose. Notably, pi-pi stacking interactions (magenta) are observed between the ligand and Phe A:83, stabilizing the aromatic ring. Additionally, pi-sulfur interaction (yellow) is formed with Met A:79, contributing to further stabilization through interaction with the sulfur atom in the binding pocket. Pi-pi T-shaped interactions are present with Tyr A:76, enhancing the binding through perpendicular interactions between aromatic rings. The alkyl and pi-alkyl interactions (light purple) involve residues like Arg A:96, Phe A:83, and Met A:79, further adding to the hydrophobic stabilization of the ligand within the binding site. van der Waals interactions (light green) between the ligand and residues such as Ser A:252, Leu A:100, His A:101, and Ala A:256 create additional weak, but significant, stabilizing forces. The presence of these interactions collectively suggests that compound 6e binds to the protein's active site through various non-covalent forces, including aromatic stacking, hydrophobic, and sulfur-based interactions. These mechanisms imply that the compound may demonstrate a strong binding affinity and potential biological activity against the protein target.

3.5. ADME study

In evaluating the ADME properties of compounds **6c**, **6d**, and **6e**, the structural differences in functional groups significantly impact their pharmacokinetic characteristics (Table 4). All three compounds share a thiazole core with a pyrazole moiety substituted by distinct phenyl groups. Compound 6d contains a methoxy group (-OCH3) on the phenyl ring,

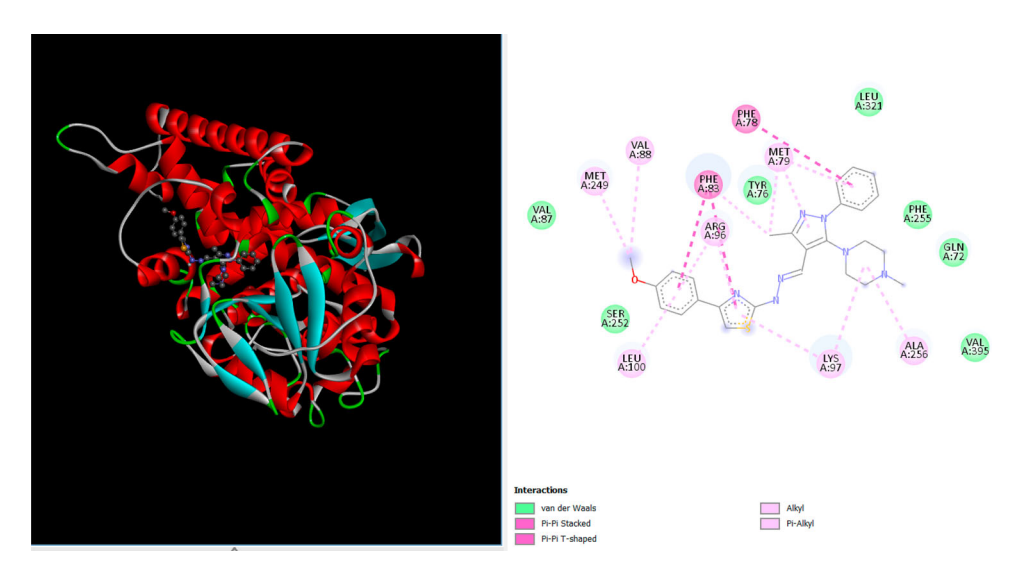


Figure 6. 3D and 2D interactions of compound 6d with target.

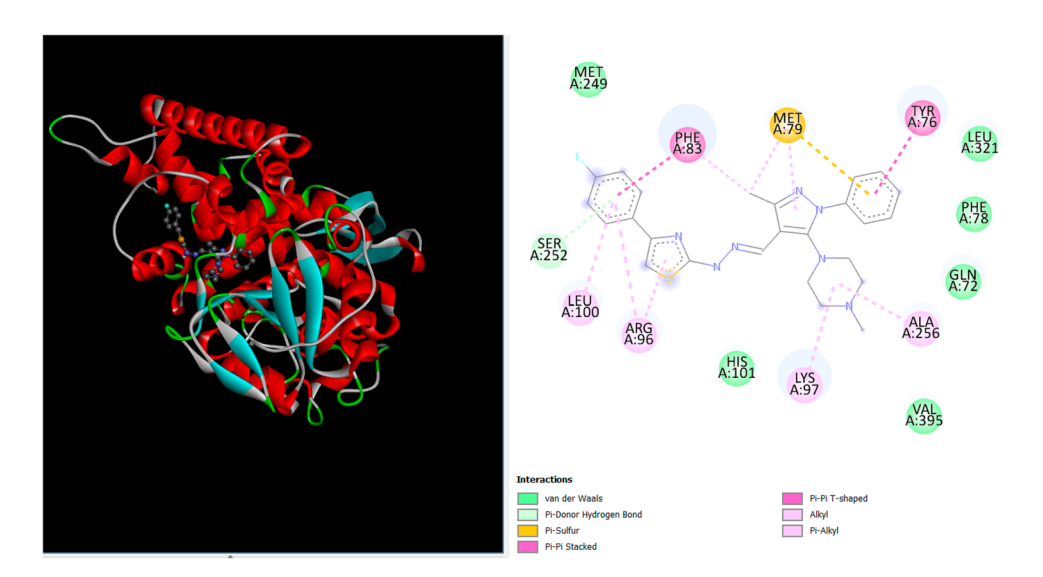


Figure 7. 3D and 2D interactions of compound 6e with target.

resulting in 35 heavy atoms, while compounds **6c** and **6e** have 34 heavy atoms due to their bromo (-Br) and fluoro (-F) groups, respectively. This variation affects molecular complexity and target interaction potential. Compound **6d** has a slightly higher fraction of Csp3 (0.27) compared to **6c** and **6e** (0.24), due to the methoxy group, which increases three-dimensional flexibility. The halogens in **6c** and **6e** contribute to their more rigid and planar structures. Flexibility, indicated by rotatable bonds, is also greater in **6d** (7 rotatable bonds) compared to **6c** and **6e** (6 each), which may enhance binding adaptability. In terms of hydrogen bonding, **6d** and **6e** each have 5 hydrogen bond acceptors, while **6c** has 4. All compounds possess one hydrogen bond donor on the hydrazone linker, essential

(i) DMF, POCl₃ and (ii) K₂CO₃, 1-methyliperazine

Scheme 1. Synthesis of 3-methyl-5-(4-methylpiperazin-1-yl)—1-phenyl-1*H*-pyrazole-4-carbaldehyde.

Scheme 2. Synthesis of piperazinyl-pyrazolyl-2-hydrazinyl thiazole derivatives.

for interacting with biological targets. The bromo group in 6c contributes to its highest molar refractivity (151.08), followed by 6d (149.87) and 6e (143.33). The topological polar surface area (TPSA) is highest for 6d (99.05 Å²) due to the methoxy group, with 6c and 6e having a TPSA of 89.82 Å². Regarding lipophilicity, 6c shows the highest log Po/w (4.63), making it more lipophilic, while 6d has the lowest (4.00). Solubility follows the same trend, with 6c being the least soluble (-6.96). All compounds exhibit good gastrointestinal absorption but are unlikely to cross the blood-brain barrier, limiting CNS effects. These compounds inhibit several cytochrome P450 enzymes, indicating potential drug-drug interactions. The compound 6d demonstrates better solubility and lower lipophilicity, while 6c and 6e are more lipophilic with reduced solubility. The comparative analysis of compounds 6c, 6d, and 6e based on their radar plots and boiled egg models reveals distinct differences in their ADME properties (Table 5). Compound 6c exhibits the highest lipid solubility, attributed to its bromo substituent, while 6d shows the lowest lipid affinity due to the methoxy group. In terms of flexibility, 6d is the most flexible with seven rotatable bonds, enhancing its potential for target interactions, whereas 6c and 6e have six rotatable bonds each. Compound 6d also has the highest polarity and topological polar surface area, benefiting solubility. All compounds indicate high gastrointestinal absorption potential, but none cross the blood-brain barrier, minimizing central nervous

Table 4.	ADME and	drug likene	ess of the	compounds	6c, 6d	and
6e.						

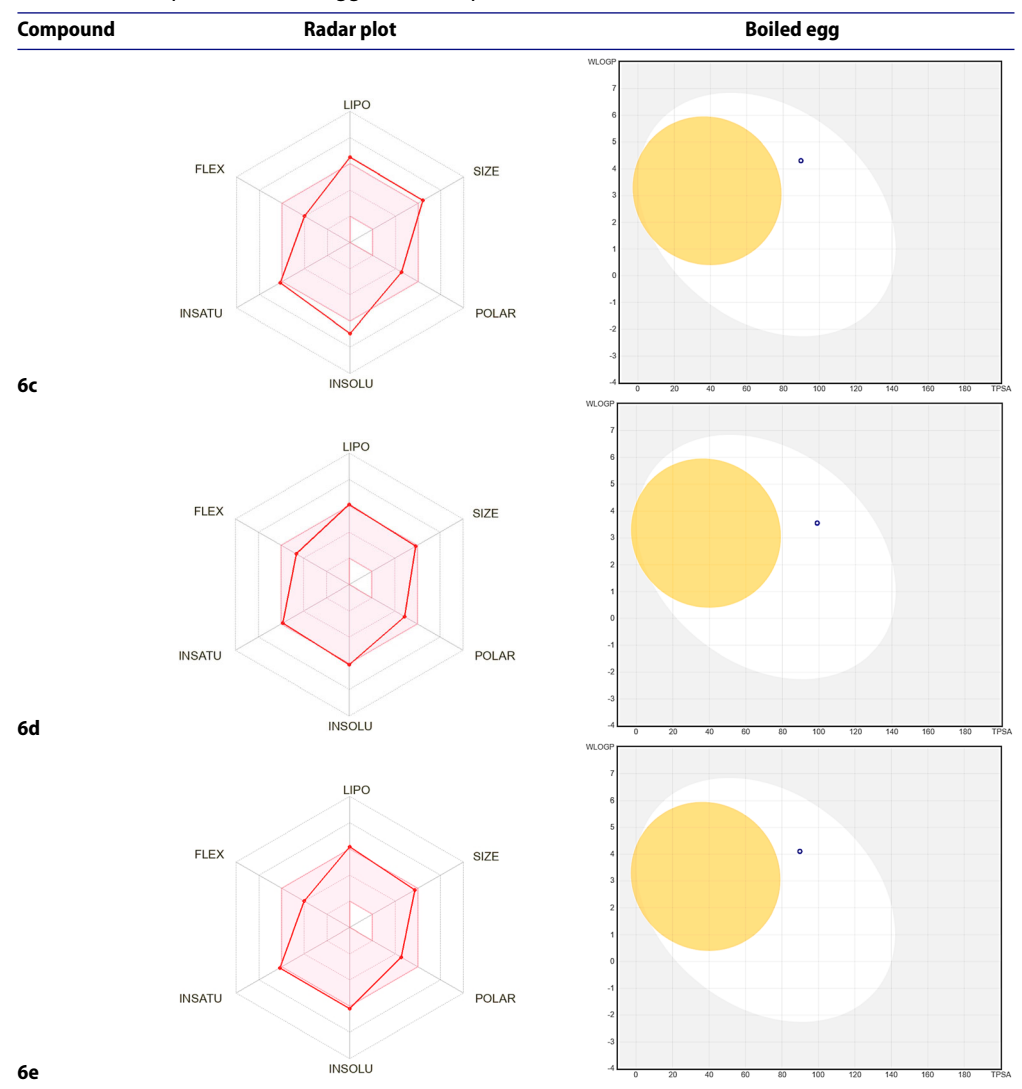
ADME parameter		Compounds	
	6с	6d	6e
Num. heavy atoms	34	35	34
Fraction Csp3	0.24	0.27	0.24
Num. rotatable bonds	6	7	6
Num. H-bond acceptors	4	5	5
Num. H-bond donors	1	1	1
Molar Refractivity	151.08	149.87	143.33
TPSA	89.82Å ²	99.05Å ²	89.82Å ²
Consensus Log Po/w	4.63	4.00	4.36
Log S (ESOL)	-6.96	-6.12	-6.21
GI absorption	High	High	High
BBB permeant	No	No	No
<i>P</i> -gp substrate	Yes	Yes	Yes
CYP1A2 inhibitor	No	No	No
CYP2C19 inhibitor	Yes	Yes	Yes
CYP2C9 inhibitor	Yes	Yes	Yes
CYP2D6 inhibitor	Yes	Yes	Yes
CYP3A4 inhibitor	Yes	Yes	Yes
Lipinski	Yes	Yes	Yes
Ghose	No	No	No
Veber	Yes	Yes	Yes
Egan	Yes	Yes	Yes
Muegge	No	No	No
Bioavailability Score	0.55	0.55	0.55

system effects. The compound **6d**'s enhanced polarity and flexibility may improve target interactions, while **6c**'s higher lipid solubility could increase absorption, making all three compounds promising candidates for further investigation in drug development.

4. Conclusion

In summary, this research efficiently developed a number of derivatives of piperazinylpyrazolyl-2-hydrazinyl thiazole and evaluated their antitubercular potential. The advanced spectroscopic methods like FT-IR, ¹H NMR, and ¹³C NMR were used to confirm the structures of nine synthesized derivatives (6a - 6i). The compounds were assessed for their anti-Mycobacterial activity against Mycobacterium tuberculosis (H37Rv strain), and compound 6c, containing a bromophenyl group, demonstrated the highest potency with a minimum inhibitory concentration (MIC) of 1.6 μg/mL. This result is comparable to standard drugs like isoniazid and ethambutol. The SAR study showed that electron-withdrawing groups - especially bromine and fluorine - were essential in increasing antitubercular efficacy. Additionally, molecular docking studies highlighted strong non-covalent interactions between 6c and its target protein, suggesting its high binding affinity. The DFT study reveals that the electronic and structural properties of compounds 6c, 6d, and 6e are significantly influenced by their substituents (bromine, methoxy, and fluorine). The variations in electron-withdrawing or donating effects alter their HOMO-LUMO energy gaps, softness, and chemical reactivity. The MESP analysis highlights the regions of electrostatic potential, which play a crucial role in molecular interactions with biological targets. Compound 6c, with its bromine substituent, shows enhanced antitubercular activity, correlating with its favorable electronic profile, as evidenced by its lower MIC value compared to 6d and

Table 5. Radar plot and Boiled egg of the compounds 6c, 6d and 6e.



6e. The ADME study revealed that **6c** possessed favorable pharmacokinetic properties, including good gastrointestinal absorption and drug-likeness. The integration of experimental and computational methods highlights compound **6c** as a promising lead for the development of new antitubercular drugs. Future research could aim at optimizing these derivatives and assessing their *in vivo* efficacy to identify more potent antitubercular agents with improved pharmacokinetic properties.

Acknowledgment

The authors gratefully acknowledge CIF, Savitribai Phule Pune University, Pune for NMR analysis of the synthesized compounds. The authors also would like to thank Research center in chemistry, Loknete Vyankatrao Hiray Arts, Science and Commerce College Panchavati, Nashik.



Disclosure statement

No potential conflict of interest was reported by the author(s).

Funding

The authors disclosed that they did not receive any grants from funding agencies for the current study endeavor, which is entirely self-funded.

ORCID

Yuvraj R. Sable http://orcid.org/0009-0005-9673-2920 Vishnu A. Adole 🕩 http://orcid.org/0000-0001-7691-7884

References

- [1] Farhat M, Cox H, Ghanem M, et al. Drug-resistant tuberculosis: a persistent global health concern. Nat Rev Microbiol. 2024: 1-19.
- [2] Mancuso G, Midiri A, De Gaetano S, et al. Tackling drug-resistant tuberculosis: new challenges from the old pathogen Mycobacterium tuberculosis. Microorganisms. 2023;11(9):2277. doi:10.3390/microorganisms11092277
- [3] Al-Asady IN, Ali JF. Virulence factors of Mycobacterium tuberculosis. J Res Appl Sci Biotech. 2023;2(3):221-237. doi:10.55544/jrasb.2.3.31
- [4] Davidson G, Davidson DU, Okoye OK, et al. Overview of tuberculosis: causes, symptoms and risk factors. Asian J Res Infect Dis. 2024;15(9):8-19. doi:10.9734/ajrid/2024/v15i9370
- [5] Chowdhury K, Ahmad R, Sinha S, et al. Multidrug-resistant TB (MDR-TB) and extensively drug-resistant TB (XDR-TB) among children: where we stand now. Cureus. 2023;15(2):e35154. doi:10.7759/cureus.35154
- [6] Vishwakarma D, Gaidhane A, Sahu S, et al. Multi-drug resistance tuberculosis (MDR-TB) challenges in India: A review. Cureus. 2023;15(12):e50222. doi:10.7759/cureus.50222
- [7] Wei X, Yue L, Zhao B, et al. Recent advances and challenges of revolutionizing drug-resistant tuberculosis treatment. Eur J Med Chem. 2024;116785.
- [8] Hazra S, Hazarika R, Patra S. Multitargeting: an alternative approach to tackle multidrug resistance in tuberculosis. Curr Drug Targets. 2023;24(9):751-775. doi:10.2174/138945012466623 0505145335
- [9] Takate SJ, Shinde AD, Karale BK, et al. Thiazolyl-pyrazole derivatives as potential antimycobacterial agents. Bioorg Med Chem Lett. 2019;29(10):1199-1202. doi:10.1016/j.bmcl.2019.03.020
- [10] Deshmukh HS, Adole VA, Kumar A, et al. Synthesis, spectroscopic (IR and NMR), HOMO-LUMO, NLO, molecular docking and ADME study of (E)-2-(2-((5-chloro-3-methyl-1phenyl-1H-pyrazol-4-yl) methylene) hydrazineyl)-4-(4-nitrophenyl) thiazole. J Mol Struct. 2024;1305:137745. doi:10.1016/j.molstruc.2024.137745
- [11] Mohamed-Ezzat RA, Omar MA, Temirak A, et al. Synthesis, biological evaluation, and docking studies of pyrazole-linked benzothiazole hybrids as promising anti-TB agents. J Mol Struct. 2024;1311:138415. doi:10.1016/j.molstruc.2024.138415
- [12] Gangurde KB, More RA, Adole VA, et al. Design, synthesis and biological evaluation of new series of benzotriazole-pyrazole clubbed thiazole hybrids as bioactive heterocycles: Antibacterial, antifungal, antioxidant, cytotoxicity study. J Mol Struct. 2024;1299:136760. doi:10.1016/j.molstruc.2023.136760
- [13] Mahmoud HK, Kassab RM, Gomha SM. Synthesis and characterization of some novel bisthiazoles. J Heterocycl Chem. 2019;56(11):3157-3163. doi:10.1002/jhet.3717
- [14] Abd El-Lateef HM, Sayed AR, Gomha SM, et al. Synthesis and study of poly [(hydrazinylazo)] thiazoles as potent corrosion inhibitors for cast iron-carbon alloy in molar HCl: A collective



- computational and experiential methods. J Mol Liq. 2021;337:116555. doi:10.1016/j.molliq.
- [15] Alshabanah LA, Gomha SM, Al-Mutabagani LA, et al. Cross-linked chitosan/multi-walled carbon nanotubes composite as ecofriendly biocatalyst for synthesis of some novel benzil bis-thiazoles. Polymers (Basel). 2021;13(11):1728. doi:10.3390/polym13111728
- [16] Khalil KD, Ahmed HA, Bashal AH, et al. Efficient, recyclable, and heterogeneous base nanocatalyst for thiazoles with a chitosan-capped calcium oxide nanocomposite. Polymers (Basel). 2022;14(16):3347. doi:10.3390/polym14163347
- [17] Said MA, Riyadh SM, Al-Kaff NS, et al. Novel Bis-thiazoles with pyridine and 1, 4-Dihydropyridine linkers as potential anti-Alzheimer agents. J Mol Struct. 2025;1322:140347. doi:10.1016/j.molstruc.2024.140347
- [18] Gomha SM, Abdelhamid AO, Abdelrehem NA, et al. Efficient synthesis of new benzofuranbased thiazoles and investigation of their cytotoxic activity against human breast carcinoma cell lines. J Heterocycl Chem. 2018;55(4):995-1001. doi:10.1002/jhet.3131
- [19] Gomha SM, Abdelhamid AO, Kandil OM, et al. Synthesis and molecular docking of some novel thiazoles and thiadiazoles incorporating pyranochromene moiety as potent anticancer agents. Mini Rev Med Chem. 2018;18(19):1670-1682. doi:10.2174/1389557518666180424113819
- [20] Sayed AR, Gomha SM, Taher EA, et al. One-pot synthesis of novel thiazoles as potential anticancer agents. Drug Des Devel Ther. 2020;120:1363-1375. doi:10.2147/DDDT.S221263
- [21] Mahmoud HK, Gomha SM, Farghaly TA, et al. Synthesis of thiazole linked imidazo [2, 1-b] thiazoles as anticancer agents. Polycyclic Aromat Compd. 2021;41(8):1608-1622. doi:10.1080/10406638.2019.1689514
- [22] Mahmoud HK, Abdelhady HA, Elaasser MM, et al. Microwave-assisted one-pot three component synthesis of some thiazolyl (hydrazonoethyl) thiazoles as potential anti-breast cancer agents. Polycyclic Aromat Compd. 2022;42(10):7232-7246. doi:10.1080/10406638.2021.199
- [23] Kassab RM, Al-Hussain SA, Abdelmonsef AH, et al. Novel xylenyl-spaced bis-thiazoles/thia zines: synthesis, biological profile as herpes simplex virus type 1 inhibitors and in silico simulations. Future Med Chem. 2024;16(1):27-41. doi:10.4155/fmc-2023-0210
- [24] Pallavi HM, Al-Ostoot FH, Kameshwar VH, et al. Design, synthesis, characterization, docking studies of novel 4-phenyl acrylamide-1, 3-thiazole derivatives as anti-inflammatory and antiulcer agents. J Mol Struct. 2023;1292:136126. doi:10.1016/j.molstruc.2023.136126
- [25] Bhanwala N, Gupta V, Chandrakar L, et al. Thiazole heterocycle: an incredible and potential scaffold in drug discovery and development of antitubercular agents. ChemistrySelect. 2023;8(46):e202302803. doi:10.1002/slct.202302803
- [26] Ouf SA, Gomha SM, Eweis M, et al. Antidermatophytic activity of some newly synthesized arylhydrazonothiazoles conjugated with monoclonal antibody. Sci Rep. 2020;10(1):20863. doi:10.1038/s41598-020-77829-x
- [27] Arshad MF, Alam A, Alshammari AA, et al. Thiazole: a versatile standalone moiety contributing to the development of various drugs and biologically active agents, Molecules. 2022;27(13):3994. doi:10.3390/molecules27133994
- [28] Ali I, Nadeem Lone M, Al-Othman Z, et al. Heterocyclic scaffolds: centrality in anticancer drug development. Curr Drug Targets. 2015;16(7):711-734. doi:10.2174/1389450116666150309 115922
- [29] Bekhit AA, Abdel-Aziem T. Design, synthesis and biological evaluation of some pyrazole derivatives as anti-inflammatory-antimicrobial agents. Bioorg Med Chem. 2004;12(8):1935-1945. doi:10.1016/j.bmc.2004.01.037
- [30] Khan MF, Alam MM, Verma G, et al. The therapeutic voyage of pyrazole and its analogs: a review. Eur J Med Chem. 2016;120:170-201. doi:10.1016/j.ejmech.2016.04.077
- [31] Takate SJ, Shinde AD, Karale BK, et al. Thiazolyl-pyrazole derivatives as potential antimycobacterial agents. Bioorg Med Chem Lett. 2019;29(10):1199-1202. doi:10.1016/j.bmcl.2019.03.020
- [32] Jadhav SB, Fatema S, Sanap G, et al. Antitubercular activity and synergistic study of novel pyrazole derivatives. J Heterocycl Chem. 2018;55(7):1634-1644. doi:10.1002/jhet.3198



- [33] Bansal KK, Bhardwaj JK, Saraf P, et al. Synthesis of thiazole clubbed pyrazole derivatives as apoptosis inducers and anti-infective agents. Materials Today Chemistry. 2020;17:100335. doi:10.1016/j.mtchem.2020.100335
- [34] Gopal PN, Poda S, Swetha BS, et al. Synthesis, charectertisation and antitubercular evaluation of pyarzoline clubbed thiazole hybrids. Curr Trends Biotechnol Pharm. 2024;18(2):1788–1797. doi:10.5530/ctbp.2024.2.27
- [35] Kuang W, Zhang H, Wang X, et al. Overcoming Mycobacterium tuberculosis through small molecule inhibitors to break down cell wall synthesis. Acta Pharmaceutica Sinica B. 2022;12(8):3201-3214. doi:10.1016/j.apsb.2022.04.014
- [36] Yan W, Zheng Y, Dou C, et al. The pathogenic mechanism of Mycobacterium tuberculosis: implication for new drug development. Mol Bio. 2022;3(1):48. doi:10.1186/s43556-022-00 106-v
- [37] Liu Y, Grimm M, Dai WT, et al. CB-Dock: A web server for cavity detection-guided protein-ligand blind docking. Acta Pharmacol Sin. 2020;41(1):138-144. doi:10.1038/s41401-019-0228-6
- [38] Beeke AD. Density-functional thermochemistry. III. The role of exact exchange. J. Chem. Phys. 1993;98(7):5648-5646. doi:10.1063/1.464913
- [39] Becke AD. A new mixing of Hartree–Fock and local density-functional theories. J Chem Phys. 1993;98(2):1372-1377. doi:10.1063/1.464304
- [40] Frisch MJ, Trucks GW, Schlegel HB, et al. Gaussian 03, revision C. 02. Wallingford (CT): Gaussian, Inc.; 2013.
- [41] Dennington RDII. (2007). II; Keith, T.; Millam, J. Gauss View, Version 4.1. 2; Semichem. Inc., Shawnee Mission, KS.
- [42] Daina A, Michielin O, Zoete V. SwissADME: a free web tool to evaluate pharmacokinetics, drug-likeness and medicinal chemistry friendliness of small molecules. Sci Rep. 2017;7(1):42717. doi:10.1038/srep42717
- [43] Sadgir NV, Adole VA, Dhonnar SL, et al. Synthesis and biological evaluation of coumarin appended thiazole hybrid heterocycles: Antibacterial and antifungal study. J Mol Struct. 2023;1293:136229. doi:10.1016/j.molstruc.2023.136229
- [44] Shinde RA, Adole VA, Jagdale BS. Synthesis, computational and antimicrobial study of 2-(2-Hydrazinyl) thiazole derivatives. J Mol Struct. 2024;1300:137096. doi:10.1016/j.molstruc.2023. 137096
- [45] Adole VA, More RA, Jagdale BS, et al. Efficient synthesis, antibacterial, antifungal, antioxidant and cytotoxicity study of 2-(2-hydrazineyl) thiazole derivatives. ChemistrySelect. 2020;5(9):2778–2786. doi:10.1002/slct.201904609
- [46] Adole VA, Danish IA, Kores JJ, et al. Computational and experimental exploration of morpholine pendent 2-hydrazineyl thiazole: Insights from DFT, ADME profiling, antifungal efficacy and molecular docking analyses. Results in Chemistry. 2025;13:101951. doi:10.1016/j.rechem.2024.101951
- [47] Gangurde KB, More RA, Adole VA, et al. Design, synthesis and biological evaluation of new series of benzotriazole-pyrazole clubbed thiazole hybrids as bioactive heterocycles: antibacterial, antifungal, antioxidant, cytotoxicity study. J Mol Struct. 2024;1299:136760. doi:10.1016/j.molstruc.2023.136760
- [48] Gangurde KB, More RA, Adole VA, et al. Synthesis, antibacterial, antifungal, antioxidant, cytotoxicity and molecular docking studies of thiazole derivatives. Res Chem. 2024;7:101380. doi:10.1016/j.rechem.2024.101380
- [49] Ram Kumar A, Selvaraj S, Azam M, et al. Spectroscopic, biological, and topological insights on lemonol as a potential anticancer agent. ACS omega. 2023;8(34):31548-31566. doi:10.1021/acsomega.3c04922
- [50] Kanagathara N, Thirunavukkarasu M, Selvaraj S, et al. Structural elucidation, solvent (polar and non-polar) effect on electronic characterization, non-covalent charge interaction nature, topology and pharmacological studies on NLO active l-argininium methanesufonate. J Mol Liq. 2023;385:122315. doi:10.1016/j.molliq.2023.122315

- [51] Jayaprakash P, Selvaraj S, Kumar AR. A new organic compound (C9H12N2O2): crystal structure, characterization, Hirshfeld surface analysis, electronic properties, NLO properties, DFT calculation and molecular docking. Solid State Sci. 2024;154: 107587. doi:10.1016/j.solidstatesciences.2024.107587
- [52] Shinde RA, Adole VA, Jagdale BS, et al. Synthesis, antibacterial and computational studies of Halo Chalcone hybrids from 1-(2, 3-Dihydrobenzo [b][1, 4] dioxin-6-yl) ethan-1-one. J Indian Chem Soc. 2021;98(4):100051. doi:10.1016/j.jics.2021.100051